The turbulent boundary layer over transverse square cavities

By L. DJENIDI, R. ELAVARASAN AND R. A. ANTONIA

Department of Mechanical Engineering, University of Newcastle, NSW, 2308, Australia

Laser-induced fluorescence (LIF) and laser Doppler velocimetry (LDV) are used to explore the structure of a turbulent boundary layer over a wall made up of two-dimensional square cavities placed transversely to the flow direction. There is strong evidence of occurrence of outflows of fluid from the cavities as well as inflows into the cavities. These events occur in a pseudo-random manner and are closely associated with the passage of near-wall quasi-streamwise vortices. These vortices and the associated low-speed streaks are similar to those found in a turbulent boundary layer over a smooth wall. It is conjectured that outflows play an important role in maintaining the level of turbulent energy in the layer and enhancing the approach towards self-preservation. Relative to a smooth wall layer, there is a discernible increase in the magnitudes of all the Reynolds stresses and a smaller streamwise variation of the local skin friction coefficient. A local maximum in the Reynolds shear stress is observed in the shear layers over the cavities.

1. Introduction

A major feature of wall turbulence is its self-sustaining nature. This implies that energy is generated by the interaction between the boundary layer and the wall to compensate for the viscous losses. The equations of motion tell us that energy is extracted from the mean flow and injected into the turbulent motion via the action of the Reynolds shear stresses. Although the actual physical mechanism by which turbulence in wall flows is sustained is not fully understood (e.g. see the collection of papers edited by Panton 1997), it is well established (e.g. Tennekes & Lumley 1972) that a source of turbulent energy is the mean shear. In the case of wall turbulence, the wall itself provides a continuous source of shear or mean vorticity through the no-slip condition. Consequently, the energy supply is likely to depend on the nature of the surface. Arguably, the resulting turbulence characteristics should in some way also reflect the nature of the surface.

Supporting this conjecture is the significant difference observed in mean velocity distributions between smooth and rough walls. The effect of the roughness is usually measured in terms of a displacement or shift of the mean velocity distribution in the logarithmic region; this shift defines the roughness function $\Delta \overline{U}$ (the overbar denotes a temporal average), which is usually normalized by the friction velocity, U_τ. However, the effect is not restricted to the mean velocity. Flow visualizations and measurements in rough-wall turbulent boundary layers (e.g. Grass 1971 – pebble roughness; Krogstad & Antonia 1994 – mesh-screen roughness) indicate significant structural changes not only near the surface but everywhere in the layer. Over the rough wall, ejections and sweeps are more intense than for a smooth wall layer. Measurements over three different types of surfaces (the so-called d-type roughness

for which $\Delta\overline{U}/U_\tau$ does not depend on the roughness height k, V-groove riblets aligned along the flow, and a k-type roughness for which $\Delta\overline{U}/U_\tau$ depends on k) reported by Antonia (1994), indicated that the Reynolds stresses are increased relative to a smooth wall, with the exception of the riblet surface when it operates in a drag-reducing mode. It was also noted that different changes to the turbulence structure occurred as a result of the different types of surface.

These observations seem to negate the hypothesis (Perry, Schofield & Joubert 1969; Townsend 1976; Raupach, Antonia & Rajagopalan 1991) that, outside the roughness sublayer, and provided the Reynolds number is large enough, the turbulent motion should be independent of the wall roughness. They also underline the inadequacy of a roughness classification scheme based solely on the effect the surface roughness has on the mean velocity profile. In this context, a detailed documentation of changes to the turbulence characteristics of the layer associated with as wide a range of surface conditions as possible seems a worthwhile long-term goal.

The main aim of the present work is to investigate the effects a rough surface have on the statistics of a turbulent boundary layer. We consider only one surface, characterized by spanwise two-dimensional square grooves or cavities regularly spaced, one cavity width apart, in the streamwise direction. The interest in this surface, referred to in the literature as a 'd-type' rough surface, stems from the possibility that the boundary layer may be exactly self-preserving (i.e. only one velocity scale and one length scale are needed to describe the behaviour of turbulence everywhere in the flow). The surface also represents a relatively small departure from a smooth wall (e.g. Liu, Kline & Johnston 1966, observed low-speed streaks on this rough wall). This particular feature can be exploited to improve our knowledge of turbulence production mechanisms in near-wall turbulent flow. From a methodological viewpoint, it is attractive to study a flow with many similarities to a turbulent boundary layer on a smooth wall, but with some important differences, for example, an apparently improved quality of self-preservation. It is also a good test of whether measurement techniques can detect differences relative to a smooth wall.

The conditions for which self-preservation can be achieved were set out by Rotta (1962). Both U_τ/U_1 and $d\delta/dx$ should be independent of x (U_1, δ and x are the free-stream velocity, boundary layer thickness and streamwise coordinate respectively). These requirements are not met by a zero-pressure-gradient boundary layer over a smooth wall (such a layer can only be approximately self-preserving) but have received some experimental support for a d-type rough wall layer (e.g. Perry *et al.* 1969; Wood & Antonia 1975; Osaka & Mochizuki 1988) albeit over a limited streamwise distance (Raupach *et al.* 1991). It may be argued that self-preservation is facilitated on a d-type rough wall layer because the cavities somehow provide an 'extra' energy input into the flow. A possible mechanism by which this may occur is investigated in this paper.

There have been several studies of a boundary layer on a d-type surface but the physics of this flow, especially the effect of the cavities on the overlying shear layer, is not clearly understood. Speculations concerning the mechanisms describing the ejections of fluid from the cavities (hereafter, this type of motion is referred to as 'outflows' to distinguish it from that associated with the smooth-wall ejections described in Kline *et al.* 1967) and their interactions with the 'outer' flow need clarification. For example, the flow visualizations of Townes & Sabersky (1966) of a turbulent boundary layer over a d-type rough wall (the spacing between the cavities was only half the cavity width) indicated that there was significant communication, albeit of an intermittent nature, between outflows and the outer flow. Townes & Sabersky suggested that the outflows were triggered by some mechanism in the outer flow.
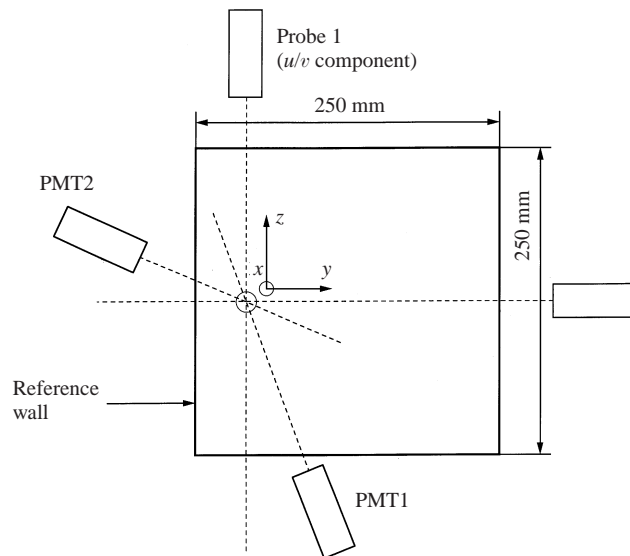
Figure 1. Rough-wall geometry.

Despite the relatively large amount of experimental data already gathered (e.g. Perry *et al.* 1969; Wood & Antonia 1975; Tani 1987; Osaka & Mochizuki 1988) for a d-type rough surface layer, near-wall data are lacking. This is mainly because hot-wire measurements are not reliable in the near-wall region. The use of laser Doppler velocimetry (LDV) should help in this respect since it allows relatively reliable estimates of the mean velocity gradient close to a smooth wall (Djenidi & Antonia 1993; Ching, Djenidi & Antonia 1995; Durst *et al.* 1996) as well as of the wall-normal stress and Reynolds shear stress (Antonia 1993).

It is not difficult to imagine that other roughnesses – including those that have been classified as 'k-type' – also interact with the outer layer although not necessarily in quite the same manner as a d-type roughness. For this reason and in view of our previously expressed reservation about the roughness classification scheme, we will refrain from using the terms d-type and k-type.

The near-surface flow is examined in some detail using LDV measurements. Flow visualizations are also used with the aim of observing the events that may contribute to the production/maintenance of turbulence on the present rough wall. Experimental details are given in §2. In §3, the wall shear stress is determined and self-preservation issues are discussed. In §4, the effects of the rough wall on the mean velocity and Reynolds stresses are investigated and discussed. The results of the flow visualization are presented in §5. Conclusions and a final discussion are given in §6.

Mainly because of the need to carry out flow visualizations, the physical size k (see figure 1) of the roughness elements was chosen to be about 5 mm, which resulted in δ/k being in the range 7 to 9. Although this ratio is small, the evidence in §4 indicates that it should not affect the way this roughness modifies the turbulence structure of the boundary layer.

2. Experimental details

The experiments were carried out in a closed-circuit constant-head vertical water tunnel. The tunnel was free of any problems arising from flow contamination, pumps,

and vibrations (see for example, Ching *et al.* 1995; Djenidi & Antonia 1995). Also, no vortex shedding frequencies were identified in measured velocity spectra (not shown here), either over the smooth wall or the rough surface.

The vertical working section (250×250 mm) was 2 m long and made of 20 mm thick Perspex. One of the working section walls was used as the rough wall – transverse 5 mm square cavities ($k/w_c = 1$, k is the height and w_c is the width of the cavity) were machined across the entire span of the wall (figure 1). The x-, y- and z-axes are in the streamwise, wall-normal and spanwise directions respectively. To trip the boundary layer, 4.5 mm high pebbles were glued onto a 30 mm wide Perspex strip, recessed into a groove 100 mm downstream from the exit of the contraction.

The Reynolds number R_θ ranged from 900 to 2300 (θ is the momentum thickness). At $R_\theta = 2300$, $k^+(kU_\tau/v)$ was about 124, indicating a fully rough turbulent layer. A three-component fibre-optic LDV system (Dantec, 5W Ar-Ion), consisting of two probes, was used in forward scatter mode. One probe measured both u, v components (two pairs of beams, each pair measuring one velocity component) while the other probe was used for measuring the w component (one pair of beams). The measuring volume dimensions were $0.047 \times 0.047 \times 0.45$ mm and $0.044 \times 0.044 \times 0.91$ mm for the two- and one-component measurements respectively. Since the measurement and physical axes were parallel to each other, it was unnecessary to apply a coordinate transformation to obtain the actual velocity components. The measurements were taken over a distance $x = 122w_c$ ($x^+ = 13313$). Since the first and second stations of measurement were only about 10δ and 20δ downstream from the turbulence triggering device, the data corresponding to those measurements are not presented. Three enhanced burst spectrum analysers (BSAs) were used for processing the photo-multiplier signals. The data rate in the outer layer ($y/\delta > 0.2$) was typically about 1500 Hz. The data rate decreased to about 50 Hz at $y^+ < 15$. About 40 000 samples were collected at each measurement point. The flow was seeded with iriodin silver particles with a nominal diameter of 2 µm. Analog outputs from the BSAs were digitized into a personal computer and stored for subsequent data reduction and analysis. The effect of the velocity bias (McLaughlin & Tiederman 1973) was corrected by weighting individual velocity realizations with the arrival time of particles in the measuring volumes. The non-uniformity of the mean velocity distribution within the measuring volume (Durst *et al.* 1992) caused an error in $\overline{U}$ no greater than 0.1%.

Flow visualizations, performed at $R_\theta = 1100$, were done with the laser-induced fluorescence (LIF) technique. A sodium fluorescein solution (2 mg/litre of water), with light absorption and emission wavelengths of 510 nm and 540 nm respectively, was injected through a 150 mm wide spanwise slot with an opening of 0.25 mm (see figure 1). The dye was introduced at a small inclination ($\simeq 5°$) to the streamwise direction and its injection rate was controlled so as to minimize any disturbance to the boundary layer. Also, a solution of rhodamine was injected through a 0.5 mm hole into a cavity at a distance of $6w_c$ downstream of the dye injection slot (see figure 1). When excited by the laser light, the rhodamine appears orange because its light emission wavelength is in the range 540–600 nm. The dye was illuminated using a combination of a 0.5 mm thick light sheet, generated from a 5W Ar-Ion laser source, and spherical and cylindrical lenses. The light sheet was either perpendicular or parallel to the surface, and views in the (x, y)- and (x, z)-planes were recorded using a CCD video camera (25 frames per second). The recorded images were processed on a Silicon Graphics workstation fitted with an Indigo^{TM} board.

Two probes, each using one pair of beams (figure 2), were used for the two-point measurements. One reference probe was fixed and the other mounted on a three-
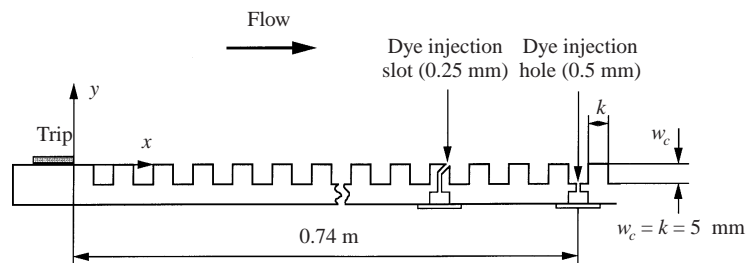
FIGURE 2. LDV configuration for two-point velocity correlation measurements.

dimensional traversing system, with a minimum displacement of $25\,\mu m$ in the x-, y- and z-directions.

3. Wall shear stress – implication for self-preservation

As mentioned earlier, the conditions for self-preservation are that $d(U_\tau/U_1)/dx$ and $d^2\delta/dx^2$ are both equal to zero. Unfortunately, the experimental determination of these two quantities, especially the first, is not straightforward. One of the main difficulties when studying rough-wall flows is the reliable determination of the effective wall shear stress. Various methods have been used; they include the momentum-integral approach (e.g. Perry *et al.* 1969), pressure-tapped roughness elements (e.g. Perry *et al.* 1969; Antonia & Luxton 1971), drag balance (e.g. Nguyen *et al.* 1990; Osaka *et al.* 1982), the combined use of the log-law and 'error in origin' (e.g. Perry & Joubert 1963), and extrapolation of the Reynolds shear stress $\overline{uv}$ (e.g. Krogstad, Antonia & Brown 1992) to the wall. Note that the existence of a log region in the mean velocity profile is questionable at low Reynolds numbers (Spalart 1988; Ching *et al.* 1995). The estimation of the total drag via the pressure-tapping method requires an independent determination of the skin friction. Perry *et al.* (1969) and Antonia & Luxton (1971) used pressure-tapped elements to estimate the total drag of rough-wall turbulent boundary layers. However, in both cases, the contribution from the viscous drag was neglected. There is no *a priori* reason why this contribution should be negligible, especially in the context of the present surface. Antonia & Luxton (1971) pointed out that an independent measurement of the viscous drag would be useful for a more complete analysis of self-preservation. In this section, we present measurements of viscous drag carried out using LDV techniques.

Figure 3 shows the streamwise distribution of the measured quantity $U_{\tau_v} = (\nu\partial\overline{U}/\partial y)^{1/2}$ (which is also a measure of the viscous drag) at $R_\theta = 1000$ over a distance of two wavelengths ($x/w_c = 4$). Over the crests, U_{τ_v} was estimated from the mean velocity gradient at the wall. Above the cavities, U_{τ_v} was deduced from measurements of $d\overline{U}/dy$ along a straight line joining the trailing and leading edges of two consecutive crests; a hypothetical U_{τ_v} was defined only for convenience. At each x-location above the crests, U_{τ_v} was estimated from a least-squares straight line fit to the near-wall $\overline{U}$ data (between 5 and 10 points were used within a distance of 0.125 mm from the crest plane). The measurements were repeated three times; the uncertainty in U_τ was about $\pm 2\%$. The same procedure was applied to estimate $d\overline{U}/dy$ along the straight line joining two crests. U_{τ_v} is maximum at the leading edge of the crest and then reduces continuously to a minimum value just before the leading edge of the next crest where the cycle recommences. The peak to trough variation is reproduced almost perfectly over the next roughness wavelength. This streamwise
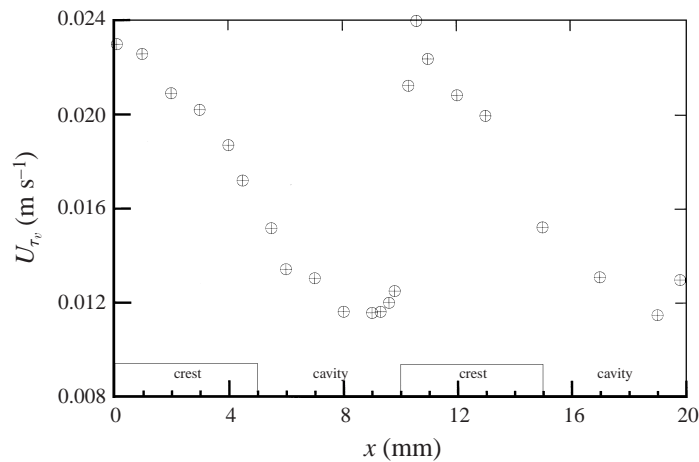
FIGURE 3. Streamwise distribution of the friction velocity over a distance of two wavelengths ($x/w = 4$).
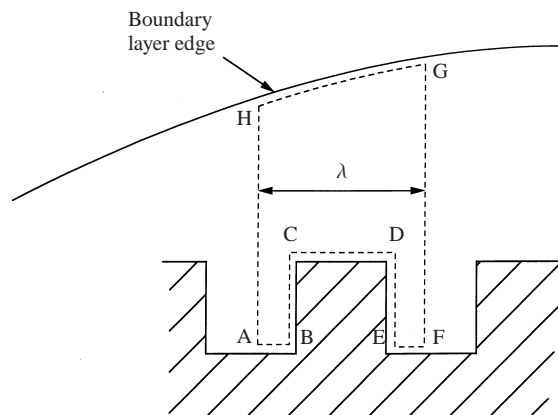

FIGURE 4. Control volume used to determine the form drag.

periodicity is similar to that observed on a wavy wall (e.g. De Angelis, Lombardi & Banerjee 1997) suggesting that the roughness elements impose some streamwise periodicity on the flow with a wavelength λ equal to that of the roughness. It also reflects a distortion of the mean velocity streamlines in the near-wall region.

The possibility of an independent determination of the viscous drag allows the form drag, which could not be measured directly, to be inferred. A control volume was defined around a single roughness element, as shown in figure 4. The friction on the vertical walls (BC and DE) of the roughness element does not contribute to the total drag. It is assumed that the friction on AB and EF (cavity bottom) represents only a small fraction of the skin friction on the top of the roughness element (CD) and can therefore be neglected. In this case, only the top of the roughness element contributes to the viscous drag. Our estimate of the viscous drag is likely to be overestimated since the present flow visualizations (and the LDV $\overline{U}$-data obtained within a cavity by Djenidi, Anselmet & Antonia 1994, figure 5) indicated that a well-defined recirculation zone occupies the full extent of the cavity, so that the skin friction should be negative along the cavity bottom. However, the slope of the velocity
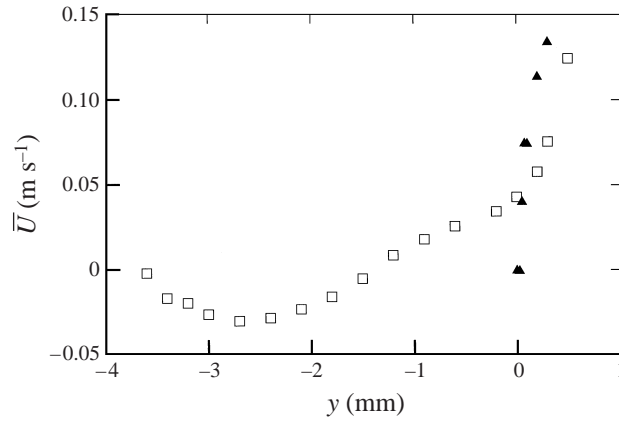
FIGURE 5. Mean velocity, within and above the cavity and above the crest (Djenidi *et al.* 1994).

profile along the bottom of the cavity suggests that neglecting the skin friction along the cavity walls cannot have any significant effect on the analysis.

Applying the momentum-integral method to the control volume yields

$$\tau = \rho U_1^2 \frac{\mathrm{d}\theta}{\mathrm{d}x} = \tau_p + \tau_v, \tag{3.1}$$

where τ is the total drag; τ_p and τ_v are the form and viscous drag acting on the roughness element. Note that self-preservation implies that $\mathrm{d}\theta/\mathrm{d}x$ is constant. Since θ is relatively easy to measure, it is convenient to determine $\mathrm{d}\theta/\mathrm{d}x$ to ascertain self-preservation.

The gradient $\mathrm{d}\theta/\mathrm{d}x$ can be determined from the measured mean velocity profiles. The form drag is then given by

$$\tau_p = \rho U_1^2 \frac{\mathrm{d}\theta}{\mathrm{d}x} - \tau_v \tag{3.2}$$

or, in terms of the friction velocity,

$$U_{\tau_p}^2 = U_\tau^2 - U_{\tau_v}^2, \tag{3.3}$$

where U_{τ_p} is the friction velocity associated with the form drag, U_τ is associated with the total drag and U_{τ_v} is associated with the viscous drag. If, as a first approximation, we assume that $\mathrm{d}\theta/\mathrm{d}x$ is constant (see figure 7), then the form drag can be inferred from (3.2). For $R_\theta = 2100$, $U_\tau = 0.022 \,\mathrm{m\,s^{-1}}$, $U_{\tau_v} = 0.011 \,\mathrm{m\,s^{-1}}$ and $U_{\tau_p} = 0.019 \,\mathrm{m\,s^{-1}}$. To estimate U_{τ_v}, we evaluated the friction acting on the roughness element crest assuming that the contributions of the sections ABC and DEF to U_{τ_v} are negligible. This estimate is assumed to represent the viscous drag acting on section ABCDEF of the control volume. The corresponding total, viscous and form drag coefficients, are $C_F = 3.9 \times 10^{-3}$, $C_{F_v} = 9.6 \times 10^{-4}$ and $C_{F_p} = 2.9 \times 10^{-3}$ respectively.

The above results suggest that the viscous drag, although smaller than the form drag, is not negligible. This result has important consequences for self-preservation which, as seen earlier, requires both U_τ/U_1 and $\mathrm{d}\delta/\mathrm{d}x$ to be independent of x. Since U_τ receives contributions from both viscous and form drags (equation (3.3)), self-preservation requires that the sum ($\tau_p + \tau_v$) should be constant. In the present case, where $\mathrm{d}P/\mathrm{d}x = 0$, even if τ_p were to remain constant, the viscous drag should decrease with x (as δ increases with x) so that $\mathrm{d}U_\tau/\mathrm{d}x < 0$. Accordingly, self-preservation would never be satisfied exactly; it could only be satisfied approximately, depending on the
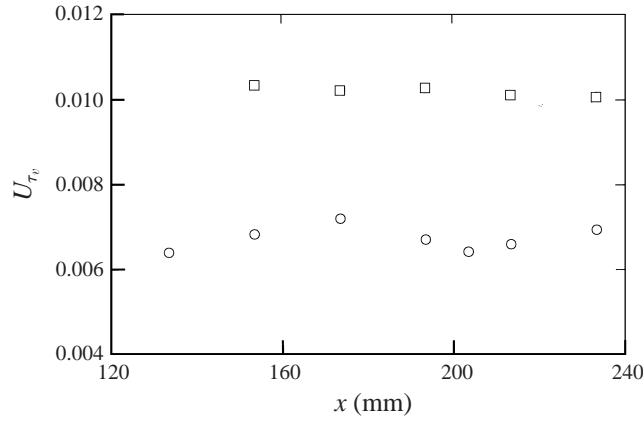
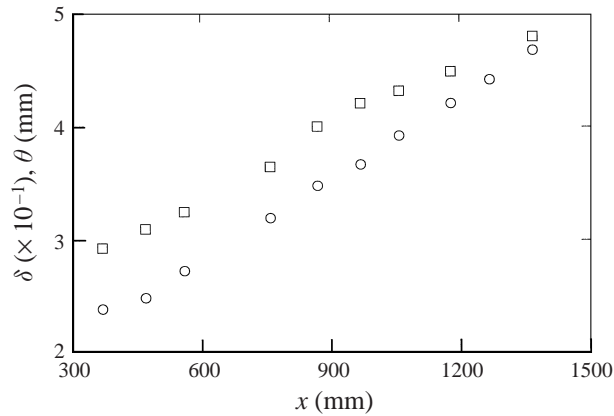FIGURE 6. Streamwise variations of U_{τ_v}. $\square$, $R_\theta = 1000$ and $\bigcirc$, $R_\theta = 2100$.

FIGURE 7. Streamwise distributions of δ ($\bigcirc$) and θ ($\square$) at $R_\theta = 2100$.

relative magnitudes of τ_p and τ_v. In rough-wall flows, τ_p can be significant compared with τ_v. It is also possible that the streamwise variation of τ_v is quite small, as can be inferred from figure 6. In this figure, the local U_{τ_v}, measured midway along the crest on several roughness elements over a streamwise distance of about $x/w_c = 21$ for $R_\theta = 1000$ and 1800, shows very little variation with x. Notwithstanding the fact that only a short range of x has been considered, it seems likely that self-preservation will be satisfied more closely than in smooth-wall layers. For the present surface, δ and θ (figure 7) appear to increase linearly with x. Note that neglecting τ_v may mask a streamwise variation in U_τ and give the impression that self-preservation is satisfied.

On the basis of the present results, one may argue that dU_τ/dx is expected to be smaller than a smooth-wall boundary layer. A physical argument that may explain this trend is the possibility that $\overline{uv}$ is maintained more effectively over the present surface than on a smooth wall since there is a natural reservoir of low-momentum fluid trapped within the cavities (this will be discussed in §4). This would facilitate the exchange of momentum between the cavities and the overlying stream which in turn would help maintain a higher turbulent energy production rate/dissipation rate ratio than for a smooth wall. This argument should also apply to other rough surfaces for which the form drag is larger than the viscous drag.
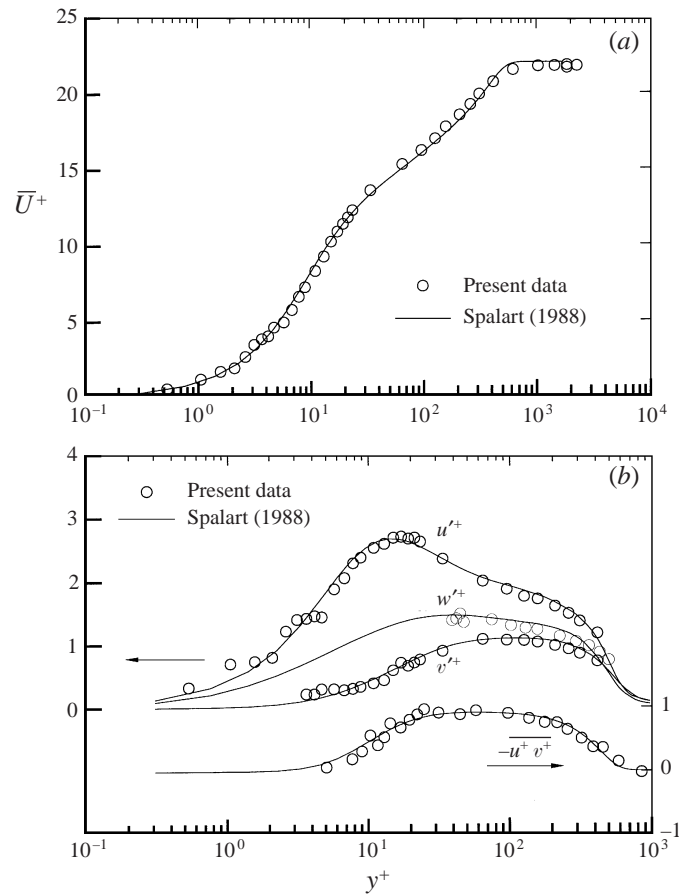
FIGURE 8. Comparison between the present LDV data δ ($\bigcirc$) and the DNS data (solid lines) of Spalart (1988) over a smooth wall.

4. Mean velocity and Reynolds stresses

It was shown in the previous section that self-preservation, although not exactly satisfied, is better approximated on the present rough surface than on a smooth wall. Speculatively, this behaviour, which indicates that the turbulent energy production process is altered, should be reflected in various turbulence statistics such as the mean velocity and the Reynolds stresses. In this section, these statistics are presented and discussed in the context of the previous speculation.

4.1. *Smooth wall*

Before considering the LDV measurements over the rough wall, it is important to assess the quality of the LDV measurements over a smooth wall. The measured normalized mean velocity distribution ($R_\theta \simeq 1400$) is compared in figure 8(*a*) with the DNS data distribution (for $R_\theta \simeq 1410$) of Spalart (1988). The friction velocity used for normalizing the data was deduced from the measured mean velocity gradient in the region $y^+ \leqslant 2.5$ (the uncertainty error was about $\pm 3\%$; for details see Djenidi & Antonia 1993). There is good agreement everywhere in the layer. Agreement of similar quality is observed (figure 8*b*) for the turbulence intensities and the Reynolds shear stress. The spanwise velocity fluctuation could not be measured below $y^+ = 30$ because
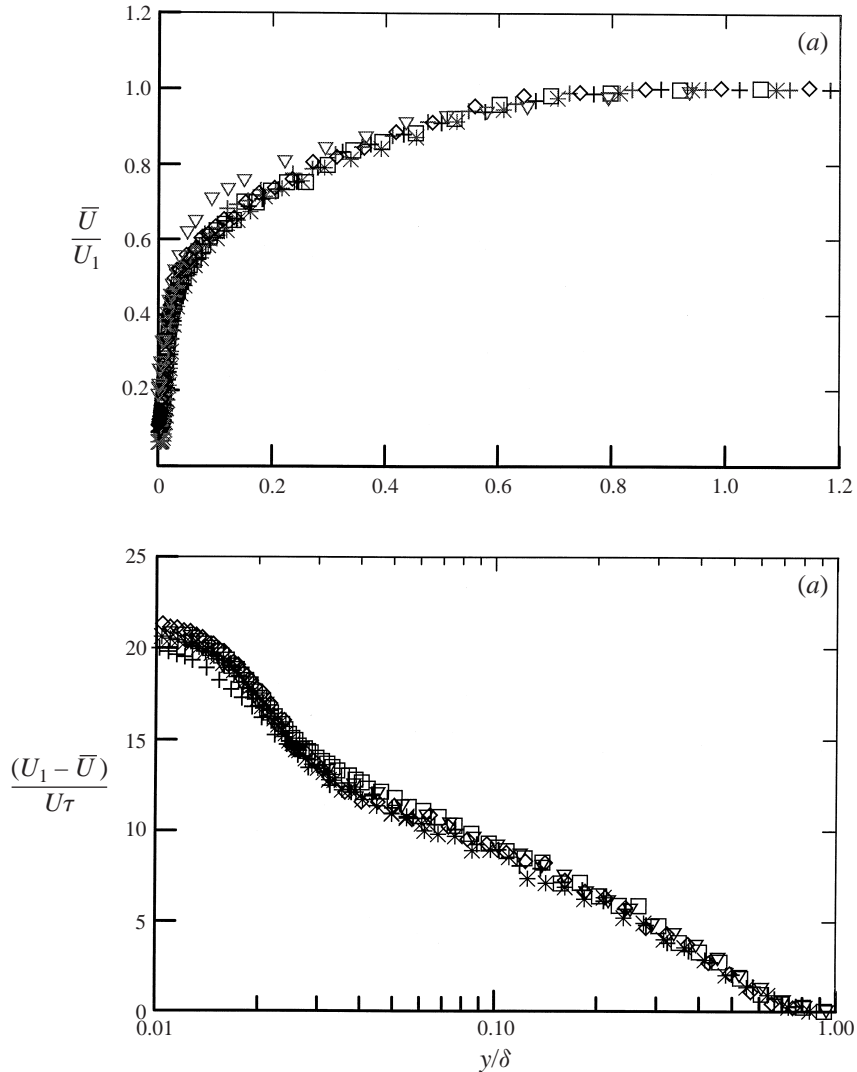
FIGURE 9. Distributions of (a) $\overline{U}/U_\tau$ and (b) $U_1 - \overline{U}/U_\tau$. *, 970 mm; +, 1060 mm; ∇, 1180 mm; $\square$, 1270 mm; $\diamond$, 1370 mm.

of the particular beam configuration that was used and the problem caused by wall reflections. The good agreement, down to the edge of the viscous sublayer (figure 8b), between the DNS and the measured profiles of $\overline{v^2}$ and $-\overline{uv}$ suggests that the LDV technique is quite suitable for correctly measuring these two quantities in the wall region of the boundary layer. The comparisons presented by Antonia (1993) indicated that the hot-wire technique yields incorrect values of $\overline{v^2}$ and $-\overline{uv}$ in the wall region.

4.2. Rough wall

Mean velocity profiles measured at several x-stations (each profile is taken above a cavity, midway between consecutive crests) are plotted in figure 9(a). Here, and in subsequent figures, the origin of the profiles is at the crest plane. No attempt was made to estimate a virtual origin for the mean velocity profiles. The distributions in figure 9(a) show that the velocity profiles can be expressed as $\overline{U}/U_1 = f(y/\delta)$. This is
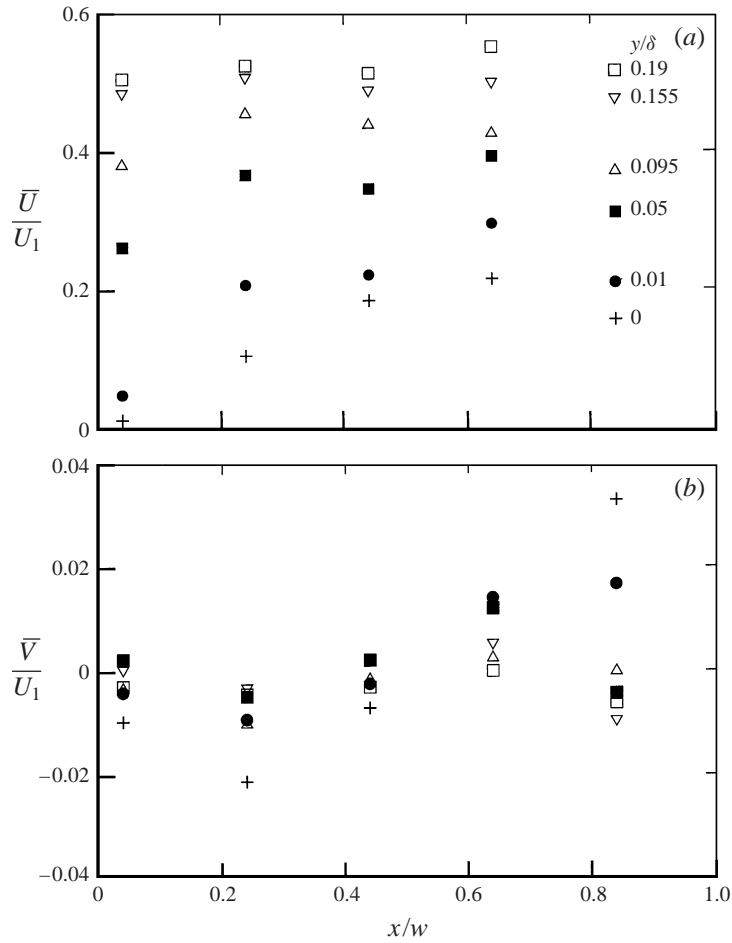
FIGURE 10. Streamwise variations of (*a*) $\overline{U}/U_1$, (*b*) $\overline{V}/U_1$ for different values of y and at $x = 1270$.

reinforced by figure 9(*b*) where $(U_1 - \overline{U})/U_\tau$ is plotted vs. y/δ; U_τ was determined in the previous section: $U_\tau = 0.022\,\mathrm{m\,s}^{-1}$. There is a reasonable collapse which can be observed down to $y/\delta \simeq 0.01$ except for the distributions at $x = 970$, 1180 and $1060\,\mathrm{mm}$ because of the uncertainty ($\Delta w/w_c = \pm 0.05$) in locating the LDV measuring volume at the same location over the cavity. The collapse – its quality is unaffected when the normalization is by U_1 instead of U_τ – is consistent with approximate self-preservation. Viscous effects preclude a collapse in the near-wall region. Note that the collapse is merely a result of self-preservation; it is not the actual theoretical condition of self-preservation, but rather a consequence of it.

Figure 10 shows streamwise variations of $\overline{U}$ and $\overline{V}$ over a cavity for values of y (y is measured above the crest plane) between 0 and $0.95\,\mathrm{mm}$. At each y, measurements were taken by displacing the LDV measuring volume along x; these measurements were repeated twice. As y increases, the waviness gradually disappears in both $\overline{U}$ and $\overline{V}$. Note the phase difference between the two components which implies that there is a contribution of the mean turbulent transport to the shear stress expressed as

$$\tau = v\frac{\partial \overline{U}}{\partial y} - \overline{uv} - \overline{U}\,\overline{V}. \tag{4.1}$$
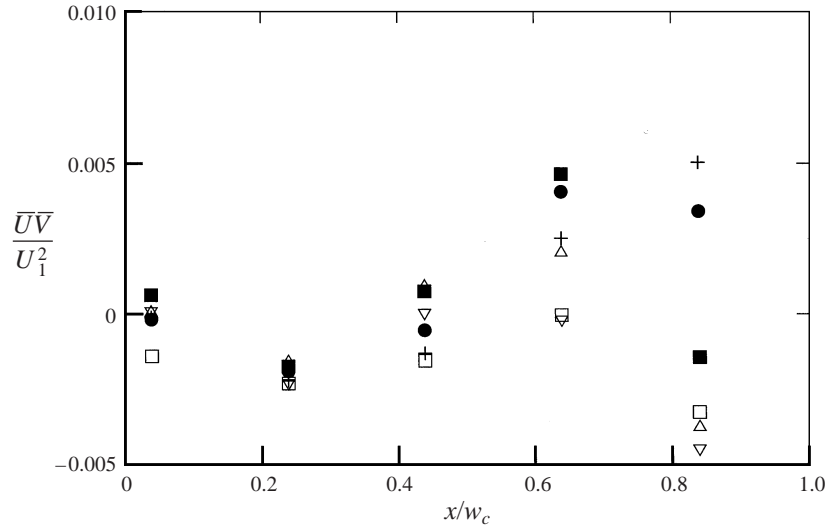
FIGURE 11. Streamwise variations of $\overline{U}\,\overline{V}/U_1^2$ for different values of y. Symbols are as in figure 10.

Since $\overline{V}$ oscillates about zero, the contribution of $(\overline{U}\,\overline{V})$ to the averaged shear stress should be small. However, it is not negligible; it is estimated that at $y \approx 0$, $\langle \overline{U}\,\overline{V} \rangle$ is about $0.33\langle \overline{uv} \rangle$, where angular brackets denote averaging over one wavelength. Figure 11 shows the $\overline{U}\,\overline{V}$ distributions calculated from the data of figure 10. There is a relatively strong streamwise variation around $\overline{U}\,\overline{V} = 0$, which diminishes as y increases. Like U_{τ_v} (figure 3), the near-wall mean velocity highlights the periodicity in the boundary condition. Perry *et al.* (1969) (see also Perry *et al.* 1987) attributed the roughness-induced streamwise distortion to a standing wave above the roughness elements. De Angelis *et al.* (1997), who studied a turbulent boundary layer over a wavy wall, also observed a similar variation in the streamlines. They argued that this is indicative of the role played by the wall in organizing or controlling the flow.

The mean streamline distortion near the roughness elements affects significantly the turbulence intensity distributions in this region (figure 12). Generally, the distortions of u', v' (the primes denote root-mean-square values) and $-\overline{uv}$ are comparable to those of $\overline{U}$, $\overline{V}$ and $\overline{U}\,\overline{V}$. Notice that while the waviness in u' and v' has significantly decreased at $y/\delta \geqslant 0.1$, it is still persistent in $\overline{uv}$. There is a significant increase in the Reynolds stresses near the downstream end of each cavity. The increase is related to the preferred occurrence of outflows and inflows in this part of the cavity. The Reynolds stresses show relatively large magnitudes, reflecting a strong boundary surface influence in the region $y/\delta \lesssim 0.02$. This influence is not limited to this region but extends to the outer region. This is verified in figure 13 which shows the Reynolds stresses normalized by U_τ^2 for the present surface and a smooth wall (Erm 1988; Erm's data, for $R_\theta \simeq 2800$, are included for reference only). The rough-wall profiles were taken at the same relative x/w_c position above several cavities covering a distance of about 14δ. All the Reynolds stresses are larger than on the smooth wall throughout the entire layer.

The magnitudes of the normalized Reynolds stresses, and particularly $-\overline{uv}$, require some discussion. The local maximum in $-\overline{uv}/U_\tau^2$ in the region $0.1 \leqslant y/\delta \leqslant 0.2$ exceeds 1 by as much as 20%. A value of $0.022\,\mathrm{m\,s^{-1}}$, deduced in the previous section from the momentum integral method, was used for U_τ. Within this region, $\overline{uv}$ is still strongly distorted by the roughness and as can be seen in figure 12(c), local values of $\overline{uv}/U_\tau^2$
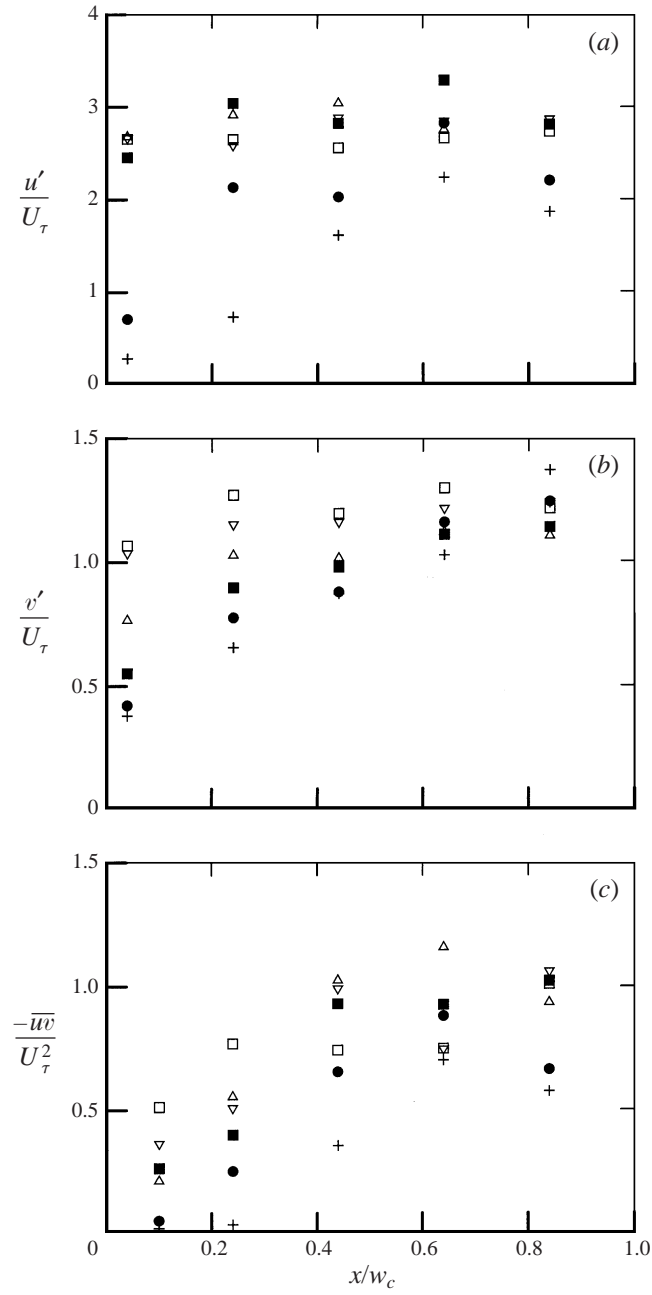
FIGURE 12. Streamwise variations of (*a*) u'/U_τ, (*b*) v'/U_τ and (*c*) $-\overline{uv}/U_\tau^2$ for different values of *y*. Symbols are as in figure 10.
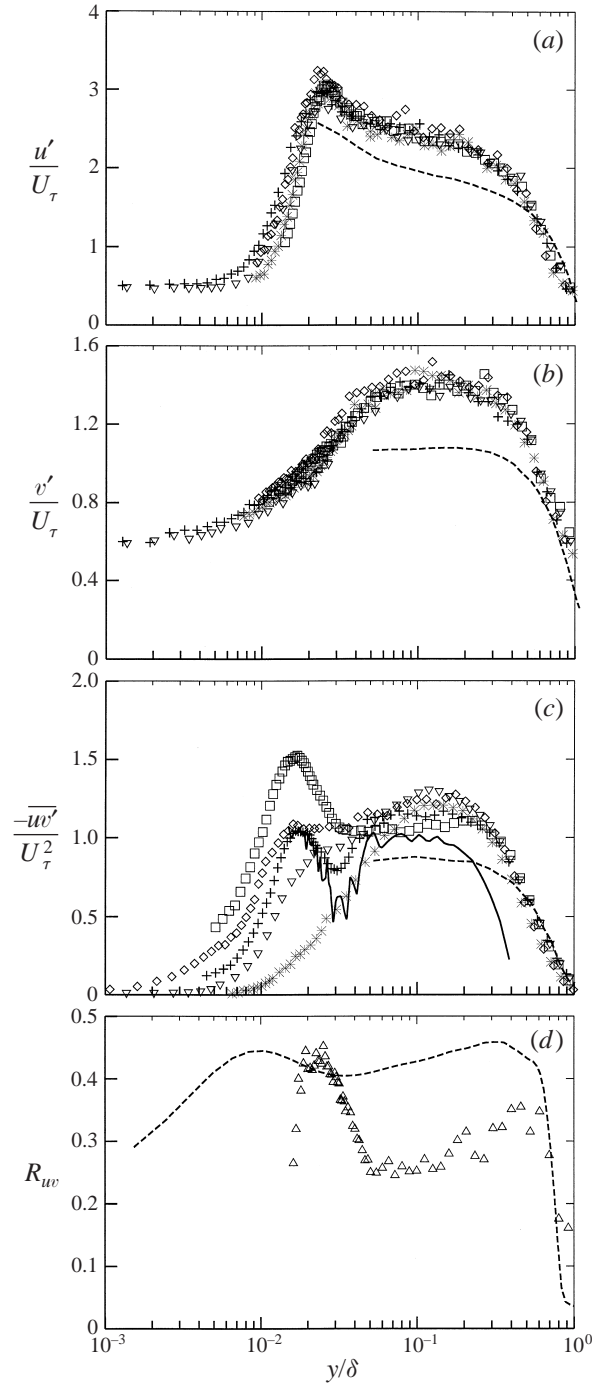
FIGURE 13. Distributions of (*a*) u'/U_τ, (*b*) v'/U_τ, (*c*) $-\overline{uv}/U_\tau^2$ and (*d*) $-\overline{uv}/\rho_{uv}$. Symbols are as in figure 4; dashed line, Erm (1988) $R_\theta \simeq 2800$. In (*c*), the solid line represents $-\overline{uv}$ calculated with (4.2), (4.3). In (*d*), only the distribution at $x = 1270\,$mm is shown with the data of Spalart (1988) (dashed line).

can be larger than 1, since U_τ represents an averaged friction velocity integrated over a wavelength. It should be pointed out that for the same nominal free-stream velocity ($U_1 \simeq 0.50\,\mathrm{m\,s^{-1}}$), all the Reynolds stresses are larger than on the smooth wall. While u' is increased by about 10%, v' and $\overline{uv}/U_\tau^2$ are increased by about 30% each, indicating that v' is more sensitive to the change in the wall condition than u'.

It should be noted that the data of Osaka *et al.* 1982; (see also Kageyama, Osaka & Nishino 1982), obtained over a similar surface, also show that, relative to a smooth wall, v' and $\overline{uv}/U_\tau^2$ are increased whereas u' is essentially unaffected. For their experiment, R_θ and δ/k were in the range 2000–7000 and 10–20 respectively. This strengthens the argument that there are genuine differences in turbulence structure between the present rough surface and a smooth wall. It is most unlikely that the differences are due to the small values of R_θ (1000–2300) and δ/k (7–9) in the present experiment. Speculatively, the magnitude of the increase is related to the strength of the outflows (see §5). In this context, the cavities can be considered as a source of low-momentum fluid. This low-momentum fluid is released, through outflows, into the outer region, contributing to the production/maintenance of $-\overline{uv}$. The production of $-\overline{uv}$ is $\overline{v^2}\mathrm{d}\overline{U}/\mathrm{d}y$, and is therefore increased as $\overline{v^2}$ is increased. It is however important to note that although $-\overline{uv}$ is increased relative to the smooth wall, the correlation coefficient, $-\overline{uv}/u'v'$, is reduced at least in the outer region of the layer (see figure 13*d*) due to the proportionately larger increase of u' and v'. There is thus a tendency for this rough-wall flow to be more isotropic than a smooth-wall flow.

For each Reynolds stress, there is relatively good collapse of distributions at different *x*-locations, further supporting the claim that self-preservation is attained, at least approximately. This is consistent with the previous results (see figures 7, 9). The $-\overline{uv}$ distributions near the wall show an unexpected local peak just above the top of the cavity ($y/\delta < 0.03$). The variation in the magnitude of the local peak reflects the uncertainty, mentioned earlier in the context of the mean velocity distributions, in locating the LDV measuring volume at precisely the same location over the cavity; a small variation in this position can result in a significant difference, as can be inferred from figure 12*c*). The local maximum is of order U_τ^2 within the region $0.01 \leqslant y/\delta \leqslant 0.03$. This local maximum can be shown to be consistent with the equation of motion (for a zero pressure gradient)

$$\overline{U}\frac{\partial \overline{U}}{\partial x} + \overline{V}\frac{\partial \overline{U}}{\partial y} = \frac{\partial}{\partial y}\left(v\frac{\partial \overline{U}}{\partial y} - \overline{uv}\right). \tag{4.2}$$

Integration of (4.2) with respect to *y* yields

$$\overline{uv} = v\left.\frac{\partial \overline{U}}{\partial y}\right|_y - v\left.\frac{\partial \overline{U}}{\partial y}\right|_{y_0} - \int_{y_0}^y \left\{\overline{U}\frac{\partial \overline{U}(s)}{\partial x} - \left(\int_{y_0}^s \frac{\partial \overline{U}(s')}{\partial x}\mathrm{d}s'\right)\frac{\partial \overline{U}(s)}{\partial s}\right\}\mathrm{d}s, \tag{4.3}$$

where the continuity equation has been used to express $\overline{V}$ in terms of $\overline{U}$; the lower limit of integration y_0 is taken at the crest plane and *s* is a dummy integration variable. In (4.3) we assumed $\overline{uv} = 0$ at $y = y_0$ which is not strictly correct (see figure 12*c*). Including its actual value in the calculation will only result in a general upward shift in the calculated distribution. To carry out the calculation, $\overline{U}$ and $\partial \overline{U}/\partial x$ need to be known. The $\overline{U}$-distribution of figure 9 was used for this purpose; for convenience $\overline{U}/U_1$ was taken as $f(\eta)$, where $\eta = y/\delta$, so that

$$\frac{\partial \overline{U}}{\partial x} = -\eta\frac{\alpha}{\delta}U_1 f'(\eta). \tag{4.4}$$
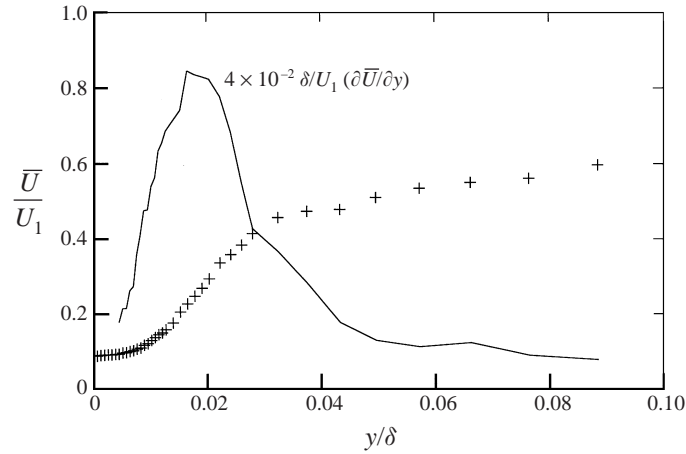
FIGURE 14. Distributions of $\overline{U}/U_1$ and $\partial\overline{U}/\partial y$ at $x = 1060\,\mathrm{mm}$.

δ is equated to αx, the value of α ($\simeq 0.024$) being determined from the data in figure 7. Substituting (4.4) into (4.3) and integrating numerically yielded the distribution shown in figure 13(c); the $\overline{U}$-profile at $x = 1060\,\mathrm{mm}$ was used in the calculation. The calculated distribution of $-\overline{uv}$ compares qualitatively well with the measured distribution at $x = 1060\,\mathrm{mm}$; in particular, the calculation reproduces the local maximum quite accurately. The assumption $\overline{U}/U_1 = f(\eta)$ may not be valid in the near-wall region where the local peak in $-\overline{uv}$ occurs. It is also likely that the left-hand side of (4.2) is negligible in the near-wall region. This would reduce (4.3) to

$$\overline{uv}\big|_{nw} = v\,\frac{\partial\overline{U}}{\partial y}\bigg|_y - v\,\frac{\partial\overline{U}}{\partial y}\bigg|_{y_0}, \tag{4.5}$$

the subscript *nw* referring to the near-wall region. The use of (4.5) to calculate $\overline{uv}$ near the wall frees the calculation from the assumption $\overline{U}/U_1 = f(\eta)$. Calculations carried out with (4.5) reproduced the local maximum with the same accuracy as with (4.3), underlining the close connection between the mean velocity profile and the local peak in $-\overline{uv}$. Indeed, (4.5) indicates that $-\overline{uv}$ follows $\partial\overline{U}/\partial y$ in the near-wall region and that a maximum in $-\overline{uv}$ should correspond to a maximum in $\partial\overline{U}/\partial y$.

A closer look (figure 14) at the near-wall region reveals that $\overline{U}$ has an inflection point ($\partial^2\overline{U}/\partial y^2 = 0$) at about the same location as that of the local maximum in $-\overline{uv}$ ($y/\delta \simeq 0.020$). The inflection point certainly results from both the adjustment of the velocity to the slip condition over the cavity and the various events occurring over the cavity (outflows, inflows). It is unlikely that such a point exists over the roughness crests. The local maximum could not have been detected using hot wires for two reasons: (i) the location of the local peak is quite close to the wall ($\sim 0.05\,\mathrm{mm}$), and (ii) the distortions to the mean flow make this technique ineffective. Note that the local maxima occur in a region of the flow where $-\overline{uv}$ would be negligible over a smooth surface. The maxima imply an increase in the mean turbulent energy production relative to a smooth wall. The relatively high values of the maxima reflect the strong correlation between u and v during outflows and inflows, underlining the strong coherence of these events. Further, two-point u-correlation measurements (figure 15) indicate that the spanwise distance, Δz^+, between low-speed streaks is about the same ($\Delta z^+ = 97$; this value is similar to that inferred earlier from flow visualizations) for
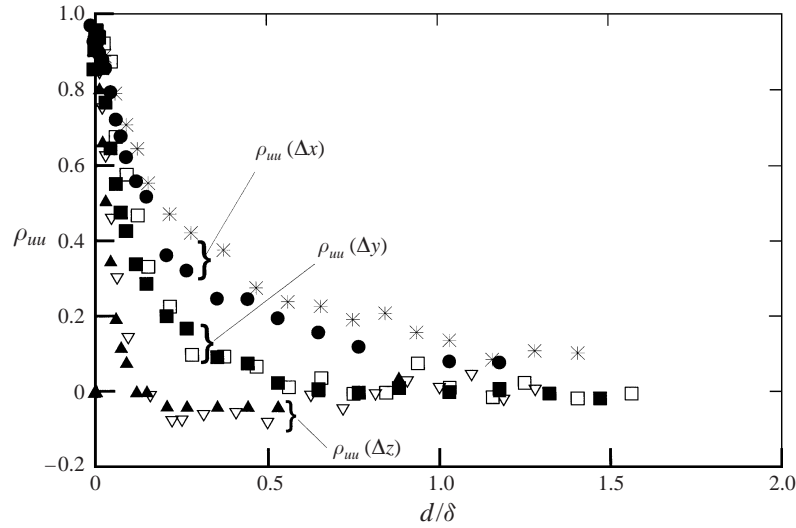
FIGURE 15. Distributions of ρ_{uu} in the x-, y- and z-directions. Closed symbols: rough wall; open symbols: smooth wall.

the two surfaces. There is a discernible reduction in the streamwise extent of the u-correlation relative to the smooth wall. In the wall-normal direction, a reduction is observed only for small separations ($d/\delta \leqslant 0.3$; d is the separation between the two measuring volumes).

It is of interest to note that a peak in $-\overline{uv}$ has been observed over a sinusoidal solid wavy boundary (height to length ratio of 0.1) by Hudson, Dykhno & Hanratty (1996). These authors noted that the loci of $(-\overline{uv})_{max}$ coincided approximately with the inflections in the mean velocity profile at the centre of the shear layer that separates from the upstream crest of the wave.

The tendency towards isotropy in the outer region can be inferred from figure 16 which is a Lumley–Newman (1977) type plot of the second ($-II \equiv \frac{1}{2}b_{ij}b_{ji}$) vs. third ($III \equiv \frac{1}{3}b_{ij}b_{jk}b_{ki}$) invariants of the Reynolds stress anisotropy tensor b_{ij}, defined as

$$b_{ij} = \frac{\overline{u_i u_j}}{\overline{q^2}} - \frac{\delta_{ij}}{3}$$

(where $u_1 \equiv u$, $u_2 \equiv v$, $u_3 \equiv w$ and $\overline{q^2} = \overline{u^2} + \overline{v^2} + \overline{w^2}$ is the turbulent energy). The inset in that figure focuses on the region $-II < 0.1$, in which all the rough-wall data lie. Since the bottom cusp ($II = III = 0$) identifies the isotropic state, the implication of this figure is clear. The invariants are smaller for the present surface (at $y/\delta = 0.02$, $-II = 0.09$, $III = 0.005$) than on a smooth wall (at $y/\delta = 0.02$, $-II = 0.15$, $III = 0.018$). The present invariants indicate however a smaller tendency towards isotropy than those obtained over a mesh-screen rough wall (the data shown in figure 16 are taken from Shafi & Antonia 1995). This suggests that the modifications due to the present roughness are less severe than those caused by the mesh-screen roughness. It also suggests that the 'interaction' between the wall and the boundary layer may be controlled, at least in part, by the wall geometry. Arguably, one can generalize this to any type of roughness. This is at variance with the generally accepted idea that, for a fully rough-wall flow, the turbulence structure is independent of the roughness geometry.
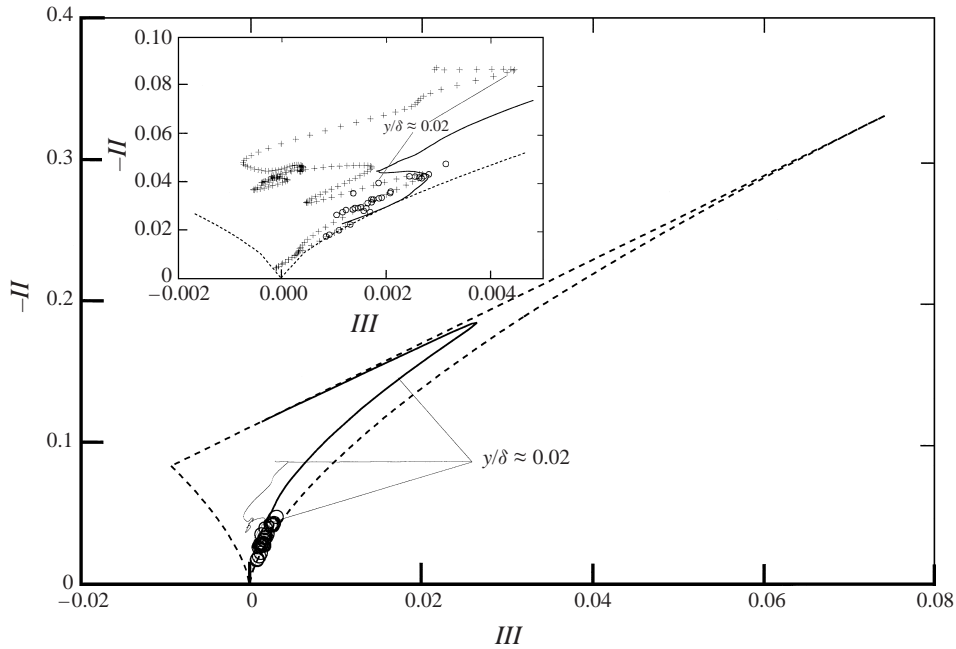
FIGURE 16. Anisotropy invariant map for the Reynolds stress tensor: +, present rough wall; ○, mesh screen rough wall (Shafi & Antonia 1995); —, smooth wall (Spalart 1988).

5. Flow visualizations

The previous sections indicated that, relative to a smooth-wall turbulent boundary layer, the Reynolds stresses are increased and self-preservation is improved. A conceptual mechanism for this has been proposed. Flow visualization is an effective way to investigate this mechanism qualitatively. Indeed, flow visualization allows events which are not easily detected by measurements to be observed. An example of the potential of this technique is illustrated in figure 17. The figure clearly shows the existence of low-speed streaks above the present rough wall; the light sheet is parallel to the wall and at a distance of 6 wall units above the crest plane (the flow is top to bottom). The appearance and break-up of the streaks are similar to what has been observed on a smooth wall (e.g. Kline *et al.* 1967). The spacing between two adjacent low-speed streaks was estimated from about 500 video frames; the mean spanwise spacing, λ^+, between streaks was about 98, with an uncertainty of $\pm 6\%$. This value is close to $100 \pm 10\%$, the average value reported over a smooth-wall (Smith & Metzler 1983). These observations imply that – relative to a smooth wall – the present surface does not disturb the flow significantly and the turbulence production process should be very similar to that for a smooth wall. However, the visualizations at a fixed spanwise location in the vicinity of the surface indicated frequent though random occurrences of three types of events:

(i) outflows from the cavities into the overlying flow;

(ii) inflows into the cavities;

(iii) periods where the overlying flow skims over the cavities with no significant exchange of fluid.

The visualization also clearly showed that there is a recirculatory motion within the cavities. The above three event categories were also observed by Townes & Sabersky
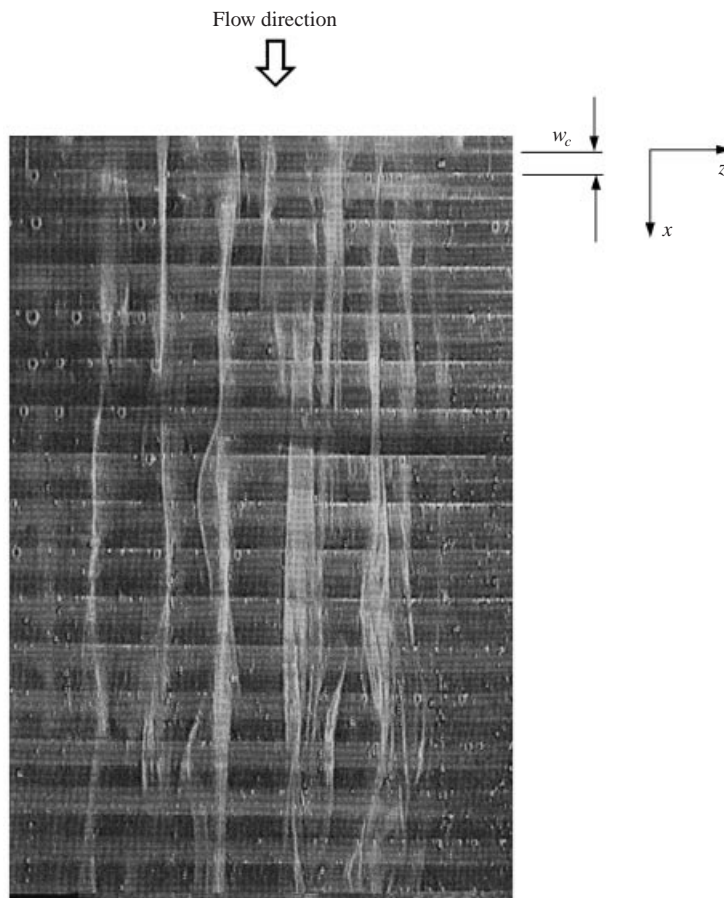
Flow direction

FIGURE 17. Low-speed streaks. The light sheet is in a plane (x, z) at a distance 6 units above the crest plane. The flow direction is indicated by the arrow.

(1966). While we cannot comment on the spatio–temporal relationships between the three categories, a few observations can be made. First, it should be pointed out that these events occur randomly not only in time but also in space. In that respect, it is clear that an outflow which occurs at a spanwise location must at the same time be balanced by one or more inflows at other spanwise positions in the groove. However, at a fixed position, an outflow is not necessarily replaced by an inflow either at an earlier or later time. Secondly, the recirculatory motion within the cavities is almost always present. Thirdly, the low-speed streaks appear to maintain their identity despite the outflows. Possibly, the (average) frequency of occurrence and intensity of the outflows may not be strong enough to perturb/destroy the low-speed streaks. Also, the length scale of the outflows may be too small compared to that of the low-speed streaks to influence them noticeably.

It was observed that outflows occur sequentially in the downstream direction: an outflow from a cavity is followed by one in the adjacent downstream cavity. It is quite difficult to determine an average distance over which this sequence takes place, but some sequences remained identifiable over about 10 cavities or a distance of 20δ.

The above sequences of outflows support the suggestion of Townes & Sabersky (1966) that the initiating mechanism for the outflows is more likely to be triggered

by the overlying flow rather than have its origin within the cavity. The visualization suggests that the outflows respond to the passage of relatively organized motions which convect in the streamwise direction. If the low-speed streaks are formed by quasi-streamwise vortices, it is plausible that these vortices also trigger the outflows. The pressure minimum at the core of these vortices could pump fluid out of the cavities. Evidence of this is observed in figure 18. A solution of diluted rhodamine was locally injected through a 0.5 mm hole located at the centre of the cavity bottom wall. When excited by the light sheet, the rhodamine turns orange. In figure 18(*a*), the rhodamine appears as a faint orange patch because it is below the plane of the light sheet, seemingly undisturbed by the flow over the cavity. As a streak passes over, the bright orange colour of the rhodamine which is now in the illuminated light plane (18*b* and 18*c*) identifies an outflow. The ejected fluid is then convected in the streamwise direction (18*d*–18*f*). Further support for this is obtained by viewing in a plane at 135° to the positive *x*-direction (figure 19). The mushroom-like structure, which is a cross-section of a low-speed streak, appears to be a characteristic signature of the quasi-streamwise vortices. The rhodamine is pumped out of the cavity by this structure (figure 19*b*). When there is no low-speed streak, the dye is undisturbed (figure 19*a*).

Flow visualizations (not shown here) using two laser sheets parallel to each other and orthogonal to the wall were carried out. The sheets were separated by a spanwise distance of 0.2δ. When an outflow was visible in one view, an inflow occurred in the other. This clearly indicates that along the span of the cavities, outflows alternate with inflows, which is consistent with the existence of alternating the low-speed and high-speed streaks in the spanwise direction. It was estimated that an outflow has a spanwise distance of the order of 100 wall units ($\approx 0.15\delta$). This is consistent with outflows triggered by pressure fluctuations associated with the near-wall quasi-streamwise vortices. It is inconsistent with Townsend's (1976) conjecture, for this particular surface, that 'large-scale pressure fluctuations can lead to simultaneous ejections of the stagnant fluid over areas comparable with the flow width' (Townsend made this comment in the context of a channel flow; the flow width is the channel height). Townsend described the pressure fluctuations as resulting from large-scale structures in the outer region of the flow and argued that the effect of the roughness on the flow depends on the channel height.

The present observations appear to raise some doubt on the commonly accepted view that, for this surface, the roughness function $\Delta \overline{U}/U_\tau$ scales only on δ or some other length-scale parameter (see Perry *et al.* 1969). The present visualizations indicate that the boundary condition is critical in organizing the near-wall flow. For example, the visualizations showed that the scale of the outflows is of the same order as the size of the cavity implying that outflows may impose a new length scale on the boundary layer. It seems therefore plausible that $\Delta \overline{U}/U_\tau$ may also scale on the roughness height. This would be consistent with the results of Townes & Sabersky (1966) which show that a Strouhal number defined by $S = kf/U_\tau$, where f is essentially the event frequency, scales on k. The data of Wood & Antonia (1975) indicated that a dependence of $\Delta \overline{U}/U_\tau$ on kU_τ/ν could not be ruled out. There is further support of this from the data of Osaka & Mochizuki (1988). Clearly, a detailed investigation of how $\Delta \overline{U}/U_\tau$ depends on kU_τ/ν and/or $\delta U_\tau/\nu$ is needed; this is however outside the scope of the present study which is mainly aimed at exploring the mechanism that facilitates self-preservation on the present surface. It seems reasonable to infer from the above discussion that the effect of the roughness on the flow depends on both δ and k. Townsend (1976) did not rule out this latter possibility since he noted that 'the
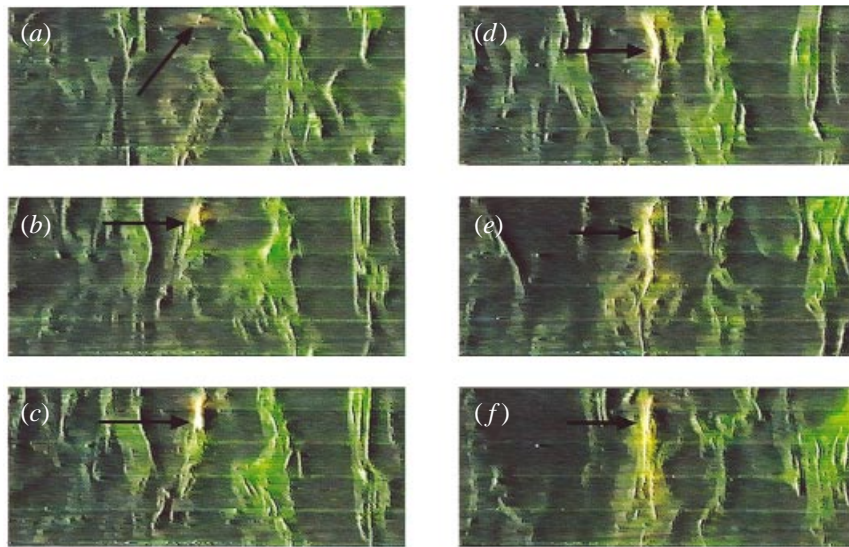
FIGURE 18. Views in the (x, z)-plane showing an outflow (marked by the orange dye) triggered by a low-speed streak.
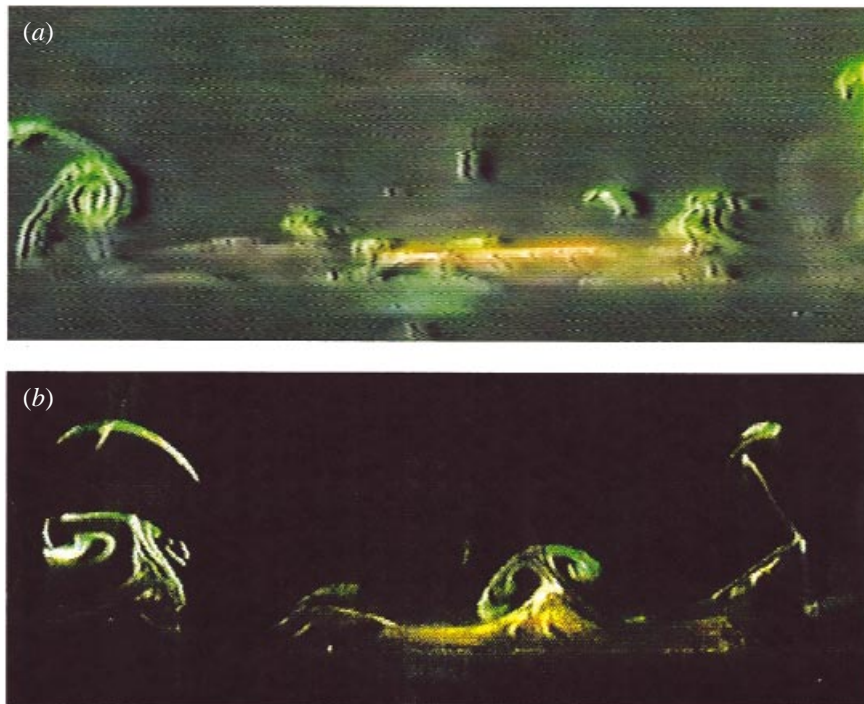

FIGURE 19. View in the plane at 135° to the positive x-direction. The mushroom-like structure, apparently a signature of the quasi-streamwise vortices, is seen to be pumping fluid out of the cavity.

effect of the rough surface on the turbulent flow is dependent on the channel width and not only on the dimensions of the roughness elements'.

The relatively frequent occurrence of outflows indicates that the flow is not in 'skimming' mode. This is more readily appreciated by viewing the video. Osaka *et al.* (1982) also observed, for a similar surface, considerable exchange of fluid between the cavities and the external flow.

6. Conclusions and discussion

LDV measurements and flow visualizations were carried out in a turbulent boundary layer over two-dimensional square cavities placed in a transverse direction to the flow and spaced one cavity width apart in the x-direction. The visualizations revealed that outflows from the cavities into the overlying flow take place randomly and are associated with the passage of near-wall quasi-streamwise vortices, similar to those found in a smooth-wall turbulent boundary layer. Along the span of the cavities, outflows alternate with inflows, consistent with the alternating low-speed and high-speed streaks. This underlines the local nature of the outflows (an outflow occurs over a distance of about w_c in the streamwise direction but less than w_c in the spanwise direction). Although the intensity of the outflows has not been quantified, it is likely that they play an important role in producing/maintaining $-\overline{uv}$ by exchanging momentum between the cavities and the layer. This is confirmed by the increase in the measured turbulence intensities and Reynolds shear stress. Further, the low-momentum fluid residing in the cavities and released during outflows may provide the right level of momentum transfer to ensure energy equilibrium. This in turn enhances self-preservation which appears to be more closely satisfied than on a smooth wall, highlighting the importance of the outflows in the process of energy production. Evidence for improved self-preservation can be found in the almost linear streamwise variation of δ and θ (determined from the mean velocity distributions), and the relatively good collapse of the u'/U_τ, v'/U_τ and $-\overline{uv}/U_\tau^2$ distributions (figure 19).

However, while self-preservation is satisfied to a close approximation on this surface (where $\mathrm{d}P/\mathrm{d}x = u$), it is likely not to be exact since $\mathrm{d}U_\tau/\mathrm{d}x = 0$ cannot be satisfied exactly. Indeed, since U_{τ_v}, which contributes to U_τ (see (3.3)), must decrease with x, U_τ cannot be constant as it is not possible for the form drag to increase with x. In the present experiment, where the Reynolds number is relatively low, the viscous component of the wall shear stress represents a significant fraction of U_τ. It is obviously important to repeat the present measurements at significantly larger Reynolds numbers. It may be surmised that boundary layers over rough surfaces, for which the form drag is the dominant contributor to U_τ, are likely to satisfy self-preservation more closely than those over a smooth wall.

The suggestion that outflows play a role in the mean energy production rate is consistent with the idea that the mechanism for sustaining the turbulence is closely related to the vorticity generation. Through the upward displacement of the trapped low-momentum fluid, outflows are a form of vorticity generation, indirectly through the formation of shear layers or directly, for example through the formation and migration of horseshoe or hairpin-like vortices. In this respect, it appears important to consider the surface conditions when studying wall turbulence and in particular motions which are responsible for the production and maintenance of $-\overline{uv}$. One should examine whether and how the outer part of the layer responds to the surface change. In the present case, the LDV measurements showed that the Reynolds stresses are

increased over the rough wall relative to a smooth wall. This suggests that the effects of the surface condition are not solely limited to the inner region of the layer but are spread out in the outer part. It is likely that changing the separation and/or the width of the present cavities will affect the outflows resulting in a modified statistical turbulent field (mean velocity, Reynolds shear stresses). It is possible that the level of interaction between the near-wall region and the outer flow will change in a manner that reflects the magnitude of the disturbance to either the near-wall region or the outer region. Consequently, the large-scale organized motion in the outer part of the flow may not be universal. While the same basic ingredients (possibly asymmetric horseshoe-like, hairpin-like or inverted double-cone vortices) may be present in each case, the size, shape and strength of the vortices are likely to depend on the details of the surface. Each boundary condition would thus leave its own signature on the structure of the outer layer.

The LDV measurements revealed a new feature in the Reynolds shear stress distributions; namely $\overline{uv}$ exhibited a local peak just above the cavity. This was attributed to the relatively strong coherent events (inflows and outflows) in this region. The measurements also showed that the periodic nature of the wall caused the friction velocity and mean streamlines to be wavy with a wavelength comparable to that of the roughness wavelength. The Reynolds stresses also displayed a streamwise periodic variation, the amplitude of the variation diminishing rapidly with distance from the wall.

REFERENCES

ANTONIA, R. A. 1993 Direct numerical simulations and hot wire experiments: a possible way ahead? In *New Approaches and Concepts in Turbulence* (ed. T. Dracos & A. Tsinober), pp. 347–365. Birkhaüser.

ANTONIA, R. A. 1994 The effect of different types of surface conditions on a turbulent boundary layer. In *Proc. First International Conference on Flow Interaction* (ed. N. W. M. Ko & B. H. K. Lee), pp. 64–79.

ANTONIA, R. A. & LUXTON, R. E. 1971 The response of a turbulent boundary layer to a step change in surface roughness. *J. Fluid Mech.* **48**, 721–761.

CHING, C. Y., DJENIDI, L. & ANTONIA, R. A. 1995 Low Reynolds number effects in a turbulent boundary layer. *Exps. Fluids* **19**, 61–68.

DE ANGELIS, V., LOMBARDI, P. & BANERJEE, S. 1997 Direct numerical simulation of turbulent flow over a wavy wall. *Phys. Fluids* **9**, 2429–2442.

DJENIDI, L., ANSELMET, F. & ANTONIA, R. A. 1994 LDA measurements in a turbulent boundry layer over a d-type rough wall. *Exps. Fluids* **16**, 323–329.

DJENIDI, L. & ANTONIA, R. A. 1993 LDA measurements in a low Reynolds number turbulent boundary layer. *Exps. Fluids* **14**, 280–288. (Erratum, *Exps. Fluids* **15**, 1993, 386.)

DJENIDI, L. & ANTONIA, R. A. 1995 LDA measurements: Power spectra estimation. *Dantec Information* **14**, 12–15.

DURST, F., KIKURA, I., LIKAKIS, I., JOVANOVIC, J. & YE, Q. 1996 Wall shear stress determination from near-wall mean velocity data in turbulent pipe and channel flows. *Exps. Fluids* **20**, 417–428.

DURST, F., MARTINUZZI, R., SENDER, J. & THEVENIN, D. 1992 LDA measurements of mean velocity, r.m.s.-values and higher order moments of turbulence intensity fluctuations in flow fields with strong velocity gradients. In *Proc. Sixth Intl Symp. on Application of Laser Techniques to Fluid Mechanics, Lisbon*, pp. 5.1.1–5.1.6.

ERM, L. P. 1988 Low Reynolds number turbulent boundary layers. PhD thesis, University of Melbourne.

GRASS, A. J. 1971 Structure features of turbulent flow over smooth and rough boundaries. *J. Fluid Mech.* **50**, 233–255.

HUDSON, J. D., DYKHNO, L. & HANRATTY, T. J. 1996 Turbulence production in flow over a wavy wall. *Exps. Fluids* **20**, 257–265.

LIU, C. K., KLINE, S. J. & JOHNSTON, J. P. 1966 An experimental study of turbulent boundary layer on rough walls. *Rep.* MD-15. Thermosciences Division, Stanford University.

KAGEYAMA, Y., OSAKA, H. & NISHINO, T. 1982 Turbulence quantities of a turbulent boundary layer over a d-type rough surface, *Mem. Faculty of Engng, Yamaguchi Univ.* **33**, 17–24.

KLINE, S. J., REYNOLDS, W. C., SCHRAUB, F. A. & RUNSTADLER, P. W. 1967 The structure of turbulent boundary layers. *J. Fluid Mech.* **30**, 741–773.

KROGSTAD, P. Å. & ANTONIA, R. A. 1994 Structure of turbulent bundary layers on smooth and rough walls. *J. Fluid Mech.* **277**, 1–21.

KROGSTAD, P. Å., ANTONIA, R. A. & BROWN, L. W. B. 1992 Comparison between rough- and smooth-wall boundary layers. *J. Fluid Mech.* **245**, 599–617.

LUMLEY, J. L. & NEWMAN, G. R. 1997 The return to isotropy of homogeneous turbulence. *J. Fluid Mech.* **82**, 161–178.

MCLAUGHLIN, D. K. & TIEDERMAN, W. G. 1973 Biasing correction for individual realization of laser anemometer measurements in turbulent flows. *Phys. Fluids* **16**, 2082–2088.

NGUYEN, V. D., DICKINSON, J., JEAN, Y., CHALIFOUR, Y., SMAILI, A., PAGE, A. & PAQUET, F. 1990 Turbulent boundary layer over a ribleted surface with tandem manipulators using surface drag balances. In *Turbulence Control by Passive Means: Proc. Fourth Eur. Drag Reduction Meeting* (ed. E. Coustols), pp. 159–172.

OSAKA, H. & MOCHIZUKI, S. 1988 Coherent structure of a d-type rough wall boundary layer. In *Transport Phenomena in Turbulent Flows: Theory, Experiments and Numerical Simulations* (ed. H. Hirata & N. Kasagi), pp. 199–211. Hemisphere.

OSAKA, H., NISHINO, T., OYAMA, S. & KAGEYAMA, Y. 1982 Self-preservation for a turbulent boundary layer over a d-type rough surface. *Trans. Japan Soc. Mech. Engng* **33**, 9–16.

PANTON, R. (Ed.) 1997 *Self-Sustaining Mechanism of Wall Turbulence*. Southampton, Computational Mech. Pubs.

PERRY, A. E. & JOUBERT, P. N. 1963 Rough wall boundary layers in an adverse pressure gradient. *J. Fluid Mech.* **17**, 193–211.

PERRY, A. E., LIM, K. L. & HENBEST, S. M. 1987 An experimental study of the turbulence structure in smooth- and rough-wall boundary layers. *J. Fluid Mech.* **177**, 437–466.

PERRY, A. E., SCHOFIELD, W. H. & JOUBERT, P. N. 1969 Rough wall turbulent boundary layer. *J. Fluid Mech.* **177**, 383–413.

RAUPACH, M. R., ANTONIA, R. A. & RAJAGOPALAN, S. 1991 Rough wall turbulent boundary layers. *Appl. Mech. Rev.* **44**, 1–25.

ROTTA, J. C. 1962 Turbulent boundary layer in incompressible flow. In *Progress in Aeronautical Science* (ed. A. Ferrie, D. Kucheman & L. H. G. Stone), pp. 1–220. Pergamon.

SHAFI, H. S. & ANTONIA, R. A. 1995 Anisotropy of the Reynolds stresses in a turbulent boundary layer over a rough wall. *Exps. Fluids* **18**, 213–215.

SMITH, C. R. & METZLER, S. P. 1983 The characteristics of low-speed streaks in the near-wall region of a turbulent boundary layer. *J. Fluid Mech.* **129**, 27–54.

SPALART, P. R. 1988 Direct numerical simulation of a turbulent boundary layer up to $R_\theta = 1410$. *J. Fluid Mech.* **187**, 61–98.

TANI, I. 1987 Turbulent boundary layer development over rough surfaces. In *Perspectives in Turbulent Studies* (ed. H. U. Meier & P. Bradshaw), pp. 223–249. Springer.

TANTIRIGE, S. C., IRIBARNE, A. P., OJHAS, M. & TRASS, O. 1994 The turbulent boundary layer over single V-shaped cavities. *Intl J. Heat Mass Transfer* **37**, 2261–2271.

TENNEKES, H. & LUMLEY, J. L. 1972 *A First Course in Turbulence*. MIT Press.

TOWNES, H. W. & SABERSKY, R. H. 1966 Experiments on the flow over a rough surface. *Intl J. Heat Mass Transfer* **9**, 729–738.

TOWNSEND, A. A. 1976 *The Structure of Turbulent Shear Flow*. Cambridge University Press.

WOOD, D. H. & ANTONIA, R. A. 1975 Measurements in a turbulent boundary layer over a d-type surface roughness. *J. Appl. Mech.* **42**, 591–597.